J. Comp. App. Res. Mech. Eng. Vol. 15. No. 1, pp. 17-38, 2025 *DOI: 10.22061/jcarme.2025.11546.2542*

Journal of Computational and Applied Research in Mechanical Engineering
jcarme.sru.ac.ir
SRTTU
JCARME
ISSN: 2228-7922

Research paper

Design and fabrication of an exoskeleton for the rehabilitation of hand fingers

B. Sarikhani[a], M. A. Ahmadi-Pajouh[b,*], A. Kolivand[a] and F. Bakhtiari-Nejad[a]

[a]*Mechanical Engineering Department, Amirkabir University of Technology, Tehran, Iran.*
[b]*Biomedical Engineering Department, Amirkabir University of Technology, Tehran, Iran.*

Article info:

Article history:

Received: 31/122024
Revised: 11/11/2025
Accepted: 14/11/2025
Online: 16/11/2025

Keywords:

Exoskeleton,
Finger rehabilitation,
Continuous passive motion exoskeleton,
Tendon based,
Finger kinematics.

***Corresponding author:**
pajouh@aut.ac.ir

Abstract

The hand plays a crucial role in daily activities; injury or paralysis significantly reduces independence. Therefore, robotic hand exoskeletons have been developed to restore motor function safely and effectively. Considering the major role of the hand in daily activities, many researchers have been working on hand rehabilitation exoskeletons. This research presents the design and implementation of a tendon-driven exoskeleton for finger rehabilitation. Continuous passive motion devices are used to maintain and restore the range of motion of the joints. The exoskeleton has been designed to help patients easily perform functional tasks. To achieve this goal, an adjustable thimble mechanism with flexible filament and a finger guide was designed. Also, this design provides the necessary force to fully guide the fingers through the whole range of motion of the joints. The designed mechanism has been modeled and simulated in MATLAB software. It has also been tested on healthy human subjects. Recorded images from the index finger in a complete range of motion have been analyzed to find the finger trajectory during flexion. The metacarpophalangeal joint of the index finger in healthy subjects has a range of motion between 0 and 90 degrees, while the exoskeleton can provide a range of motion between 0 and 94 degrees. Results show that the designed exoskeleton can provide sufficient force and an acceptable range of motion for patients up to level 2 of the Ashworth scale, which is acceptable for most different and functional varieties of continuous passive motion exoskeletons.

1. Introduction

The hand is one of the most vital parts of the body, and injuries to it not only affect a person's professional activity but also disrupt daily life, often requiring assistance from others for routine tasks [1, 2].

In addition to physical disability, hand injuries cause very high psychological pressure in a person, which leads to frustration, stress, and a lack of self-confidence.

The main cause of disability in the hand is related to the weakness of the flexor and extensor muscles [3]. Also, the fingers' speed and range of motion (ROM) decrease after a

hand injury. Pain is one of the reasons for such a decrease, which also leads to a decrease in hand strength [4, 5].

Rehabilitation that involves intensive, repetitive practice of specific tasks helps improve hand function by enabling patients to consistently perform repeated movements or daily activities, which compensates for muscle weakness and enhances the control of impaired motor functions. [1, 3, 6]. So, rehabilitation is necessary to regain some lost movement and can significantly impact a person's recovery process [7]. All the studies conducted in this field have confirmed the usefulness of rehabilitation in rehabilitating a person [8]. Some studies have also shown that rehabilitation after injuries is necessary, and if not done, the injury may haunt the person for the rest of his life [2].

Due to the possibility of performing repetitive and accurate movements, robot-assisted rehabilitation can overcome the shortcomings of traditional methods and be used as an effective and reliable method [5].

Exoskeletal robotics for rehabilitation is still a relatively emerging field, but it is expanding quickly and is becoming more prevalent in therapeutic settings. In the field of clinical rehabilitation treatment, functional rehabilitation, and the auxiliary robot exoskeletal robotics have increasingly grown in importance as technical equipment, and several studies have reported the effectiveness and even the necessity of exoskeletons and rehabilitation robots [2, 4, 9, 10]. At-home therapy has been found to improve patient rehabilitation while lowering treatment costs. Compact and affordable gadgets can greatly increase therapy efficiency [11]. Recent advancements in rehabilitation technology have combined enables chronic stroke survivors to independently perform high-intensity therapy at home with minimal therapist supervision, achieving therapy rates that are an order of magnitude higher than standard clinical care [6].

Two main motion therapy methods are applied in rehabilitation, namely continuous passive motion (CPM) and continuous active motion (CAM) [7]. In the active model, the exoskeleton has an auxiliary and supportive role in the movement of patients with little ability to move their fingers, while using the passive exoskeleton, the patient cannot move his hand. CPM helps restore movement with predetermined rhythmic movements according to the patient's needs. It can be expressed more thoroughly that active hand exoskeletons generally actively apply necessary force and torque at any moment to neutralize the patient's resistant muscle tone in the fingers by using force sensors and online monitoring of motions. However, patients using passive hand exoskeletons cannot move their hands. Therefore, the task of the passive exoskeleton is to help the patient to perform repetitive movements to recover the ROM of each joint as completely as possible. While CPM's efficacy is controversial, it is still frequently used as a therapy for recovery and a preventative device [12–19]. CPM is a rehab tool to help people recover from surgery (such as flexor tendon repair), stroke, hemiplegic hand, intra-articular adhesions, and extra-articular contractures. In general, CPM is most efficient during the initial stages following surgery. CPM rehabilitation techniques have typically been applied in clinical settings [20]. Recent clinical evidence from controlled trials supports the continued use of continuous passive motion therapy in post-surgical rehabilitation protocols, demonstrating measurable improvements in joint function and patient-reported outcomes when properly implemented [21]. Active resistance motion (CAM) becomes more significant in the later rehabilitation and recovery phases [7].

Also, in terms of structural characteristics, existing hand rehabilitation systems can be broadly split into two groups: rigid exoskeleton robots [22, 23] and soft exoskeleton robots [24–27]. Rigid link structures use only the mechanism and through kinematic chains, cause finger-flexion-like motions [28]. As a result, practically every finger movement needs to be powered by a motor, which raises the system's cost and complicates the control algorithm [29]. But rigid link structures promote safe interaction due to the ability to manage forces precisely, particularly the force directions and also its structural ability to change and adapt to the hand [28]. Another

downside of the rigid exoskeleton is that each rigid connecting rod must be profoundly aligned to the joints of the human hand; otherwise, there is a considerable risk of secondary harm to the patient, negatively impacting the user experience. These hand exoskeletons have gears, rigid anchoring, and mechanical construction [23] undoubtedly enhancing the risk of harm [29]. Such mechanisms govern tendons down the palmar and dorsal sides of the fingers [30]. Like how the fingers naturally flex and extend, pulling on either tendon causes flexion and extension [28]. The compliant nature of soft robotic systems allows them to conform to body structures and compensate for joint misalignments, simplifying donning and doffing procedures while creating more natural movement patterns that are crucial for safe patient interactions during rehabilitation [31].

Existing soft exoskeletons do, however, have some drawbacks, including a heavy hand load, imprecise transmission, an excessive number of hard anchor points, and complex control procedures [29].

It should be mentioned that patients are categorized based on the severity of the damage and the rigidity of the muscles. One of the criteria of such categorization is the resistance to passive movement of the joint. The Modified Ashworth Scale (MAS) expresses this resistance. The values of the MAS vary between 0 and 4, and a full description of the different grades is shown in Table 1 [32].

The limited ability of articular cartilages to repair and regenerate, in addition to clinical observations and research conducted concerning the effects of immobility and its harmful effects on joints, was noticed by Salter and his colleagues in 1970. Salter proposed the hypothesis that CPM will facilitate the improvement of articular cartilage condition and recovery of capsules, ligaments, and tendons. Early CPMs were simple devices of noisy motors, brakes, pulleys, ropes, and several rods [8].

2. Related works

More than 140 hand exoskeletons have been developed in the past ten years alone, 48 of which were designed to help with daily tasks. However, few have been commercialized (e.g., neomano; Neofect, Korea; carbonhand; Bioservo, Sweden), and none are insured by social insurance [28].

The most prominent tendon-driven exoskeletons of the last ten years were examined, and their characteristics can be examined as follows. Exo-Glove Poly II exoskeleton causes premature hand sweating due to the use of silicone material. Also, due to the low strength of silicone, it covers a limited force range and therefore covers a low level of the MAS. In the case of the mentioned exoskeleton, the impossibility of using an exoskeleton for hands with different dimensions is also noticed, and one exoskeleton must be made for each individual [9]. Gloreha exoskeleton is not portable and is used only at home or in clinics due to the large size of its operator's box. Another important factor about this exoskeleton is the weakness in its rehabilitation capabilities regarding flexion of the fingers. Considering the power transmission mechanism designed in this exoskeleton to move the fingers using artificial tendon and tensile force only in the extension mode and compressive force in the flexion mode, we notice a weak performance in the fingers' flexion mode.

Table 1. Modified Ashworth scale [32].

Grade	Description
0	No increase in muscle tone
1	Slight increase in muscle tone, manifested by a catch and release or by minimal resistance at the end of the range of motion when the affected part(s) is moved in flexion or extension
1+	Slight increase in muscle tone, manifested by a catch, followed by minimal resistance throughout the remainder (less than half) of the ROM
2	More marked increase in muscle tone through most of the ROM, but the affected part(s) easily moved.
3	Considerable increase in muscle tone, passive movement difficult
4	Affected part(s) rigid in flexion or extension

The last point is that to use the Gloreha exoskeleton, different gloves should be used for people with different hand sizes [33]. In the case of the Columbia University exoskeleton, the device's bulky mechanism overshadows the fingers' ROM, especially at the end of flexion mode ROM [34]. Similar to the Gloreha, the Mano exoskeleton has problems in the flexion mode of the fingers and has a bulky and annoying mechanism for the patient [35].

3. Anatomical background

3.1. Joints

The joints between the phalanges are pure hinge joints. Each hand has nine joints, one related to the thumb, while the remaining eight are associated with the remaining fingers. The head of each phalanx (except the last joint) is in the shape of a spool, and the base of the next phalanx is in a way that covers the two edges of the spool. This position removes any lateral movement from the interphalangeal joints, so the phalanges can only perform two movements of flexion and extension [36].

3.2. Tendons

Each finger has two flexor tendons. One is the deep flexor tendon connected to the volar surface of the distal phalangeal bone of the finger and its function to bend the distal interphalangeal (DIP) joint. The muscle of this tendon is located in the forearm area. Another tendon is the superficial flexor tendon, which is connected to the volar surface of the middle phalanx of the finger, and its function is to bend the proximal interphalangeal (PIP) joint. The muscle of this tendon is also located in the forearm area. There is an extensor tendon on the dorsal surface of the fingers. Its task is to open and keep the phalanges in a straight position. The muscles of these tendons are also located in the forearm area. The extensor tendons pass through the back of the wrist and behind the metacarpals and reach the fingers. Thumb, index, and sometimes little finger have two extensor tendons while other two fingers have one extensor tendon. Each extensor tendon is attached to the finger's middle and distal phalanx. The extensor tendon of each finger is widened on the dorsal surface of the proximal phalanx and covers the entire dorsal surface of the bone; therefore, it is called the extensor hood in this area. The extensor tendons of the fingers pass through the dorsal surface of the metacarpals [36].

Flexor tendons of each finger pass through tunnels of strong tissue like ligaments while passing over the bone. These tunnels are called pulleys. These pulleys keep the flexor tendons close to the bone and joint and prevent them from moving away from the bone and joint during extension or flexion of the finger. There are several pulleys on the volar or anterior surface of each finger.

Flexor tendons, while passing through the anterior surface of the finger, are placed in a layer of synovial tissue called tenosinovium. The function of this synovial layer is to release synovial fluid, they facilitate the tendon's movement under the pulleys and on the bone [36]. Fig. 1 shows a view of the finger tendons.

3.3. Finger movements

Through a sequence of finger actions, including flexion, extension, abduction, adduction, and circumduction, the hand is an astounding achievement of human evolution that allows for exceptional physical skill and the ability to handle and construct items [37].

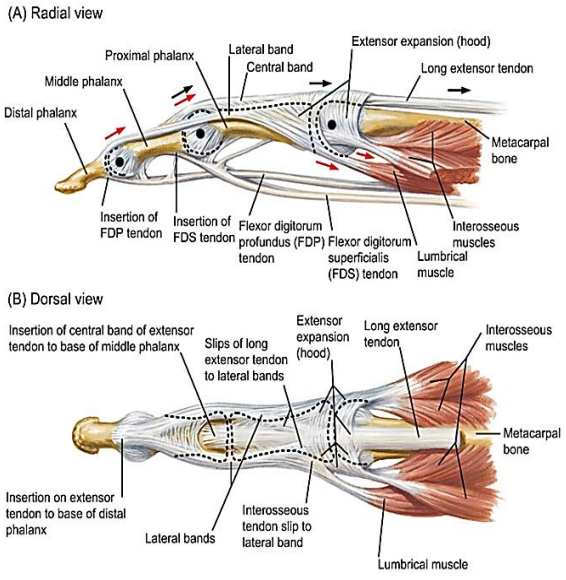

Fig. 1. The musculotendinous structure of the human finger from posterior (dorsal) and lateral (radial) view [38].

Supination is a state in which the palm is turned outwards and faces forward. Pronation is when the palm is turned inwards and towards the back. Abduction is the state of moving away from the central longitudinal axis, and adduction is its opposite state. As shown in Fig. 2, finger extension is joint motion in the opposite direction from finger flexion, which is joint motion towards the palm in relation to the standard anatomical position. Zero-degree flexion is the definition of full extension, which lines up with the back of the hand. Circumduction is defined as a circular motion of the finger [37].

4. Design

Considering the advantages and disadvantages of existing exoskeleton robots, a new passive continuous soft glove-type hand exoskeleton is proposed in this research. While tendon-driven mechanical systems provide precise force control through direct cable transmission, alternative approaches such as magnetic actuation offer potential benefits in reduced mechanical complexity and improved hygiene, though they may face limitations in generating sufficient forces for patients with higher muscle tone or larger hand sizes [39]. Considering this drawback, a tendon-driven mechanical system is designed in paper. One of the significant innovations in the exoskeleton design presented in this article is the adjustable thimble mechanism and the flexible filament finger guide, which due to this feature, the mentioned thimble can be used by patients with a variety of finger sizes. One of the other innovative features of the exoskeleton mentioned above is its significant flexibility while providing the necessary resistance to guide the fingers fully. On the other hand, with the design of the artificial tendon alignment mechanism, a unique capability has been added to the exoskeleton. This device can also be used by individuals who have lost one or two phalanges from any finger. Another important factor is that despite the relatively smaller dimensions, volume, and weight compared to similar cases, this exoskeleton can be used for patients suffering up to level 2 of the MAS, the highest level defined for the functional field of continuous passive rehabilitation exoskeletons. In addition, the control panel and complete monitoring of all parameters, from the speed and direction of movement to monitoring the amount of load on the motor, is another distinguishing feature embedded in this exoskeleton.

4.1. Distinguishing innovation compared to prior exoskeleton designs

Unlike earlier adaptive tendon-driven mechanisms [2, 3], the present design introduces a three-parameter adjustability including: (i) angular correction of the tendon alignment ($\Delta\alpha \leq 8°$), (ii) torque-to-weight ratio improvement of around 24 %, and (iii) multi-axis adaptability through an adjustable thimble allowing DOF compensation. These changes reduced trajectory error below 1° over the full 94° ROM, which had not been reported in prior CPM gloves.

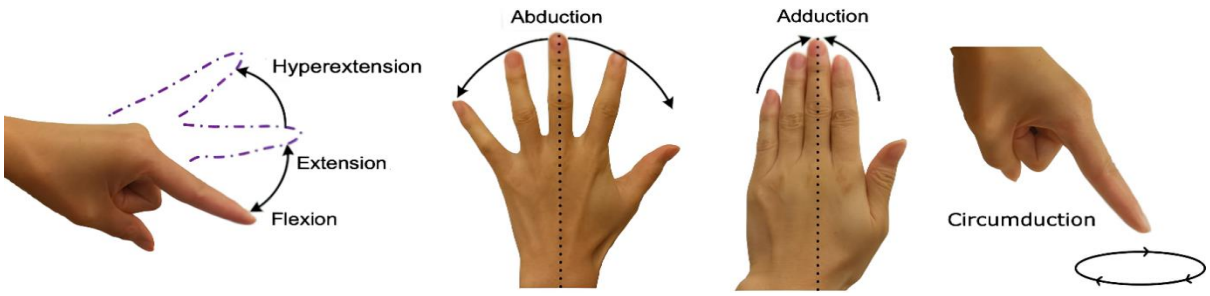

Fig. 2. Display of flexion-extension, adduction-abduction, and circumduction movements [38].

4.2. Direct and inverse kinematic analytical modeling

4.2.1. Direct kinematic model

Conforming an exoskeleton to the kinematics analysis of the fingers is one of the key considerations in designing a suitable exoskeleton. This matter was considered according to the kinematics study of Lenarsis *et al.* [40]. Since each finger of the human hand is similar to a serial robot, for the direct kinematics analysis of the index, middle, ring, and little fingers using the vector parameters and based on homogeneous matrices and Denavit-Hartenberg method, we have:

In Fig. 3, the Cartesian vectors are defined by e_1, e_2, e_3 and e_4, and the rotations corresponding to each of them are denoted by θ_1, θ_2, θ_3 and θ_4, respectively. Each finger has four degrees of freedom. The metacarpophalangeal (MCP) joint S_1 was replaced by a universal joint. The first degree of freedom represents abduction-adduction. The second degree of freedom represents the flexion-extension movement of the MCP joint. The proximal joint S_2 and the distal joint S_3 were replaced by revolute joints. All the axes of flexion and deviation of the finger joints are parallel, while the axis of rotation of the MCP joint S_1 is perpendicular to them. The length of the proximal, middle, and distal phalanges is determined by parameters l_2, l_3 and l_4, respectively.

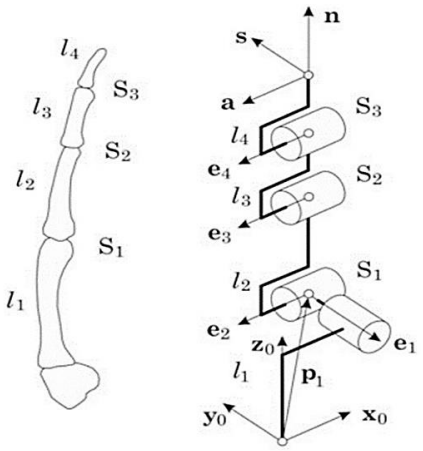

Fig. 3. Direct kinematic analysis of index, middle, ring, and little finger joints [40].

The length l_1 is a component of the existing vector p_1. x_{S1}, y_{S1} and z_{S1} describe the position of the MCP joint relative to the reference frame. The following homogeneous matrices $H_{0,1}$, $H_{1,2}$, $H_{2,3}$, $H_{3,4}$ and $H_{4,5}$ can be multiplied together to solve direct kinematics by Eqs. (1) and (2-6) [40] :

$$H = \begin{bmatrix} n^{(0)} & s^{(0)} & a^{(0)} & p^{(0)} \\ 0 & 0 & 0 & 1 \end{bmatrix} = H_{0,1}H_{1,2}H_{2,3}H_{3,4}H_{4,5} \quad (1)$$

The vectors a, s, n are the axes of the reference frame relative to the fingertip.

$$H_{0,1} = \begin{bmatrix} c_1 & 0 & -s_1 & x_{s1} \\ 0 & 1 & 0 & y_{s1} \\ s_1 & 0 & c_1 & z_{s1} \\ 0 & 0 & 0 & 1 \end{bmatrix} \quad (2)$$

$$H_{1,2} = \begin{bmatrix} 1 & 0 & 0 & 0 \\ 0 & c_2 & s_1 & 0 \\ 0 & -s_2 & c_2 & 0 \\ 0 & 0 & 0 & 1 \end{bmatrix} \quad (3)$$

$$H_{2,3} = \begin{bmatrix} 1 & 0 & 0 & 0 \\ 0 & c_3 & s_3 & 0 \\ 0 & -s_3 & c_3 & l_2 \\ 0 & 0 & 0 & 1 \end{bmatrix} \quad (4)$$

$$H_{3,4} = \begin{bmatrix} 1 & 0 & 0 & 0 \\ 0 & c_4 & s_4 & 0 \\ 0 & -s_4 & c_4 & l_3 \\ 0 & 0 & 0 & 1 \end{bmatrix} \quad (5)$$

$$H_{4,5} = \begin{bmatrix} 0 & 0 & -1 & 0 \\ 0 & 1 & 0 & 0 \\ 1 & 0 & 0 & l_4 \\ 0 & 0 & 0 & 1 \end{bmatrix} \quad (6)$$

where c_i stands for cosine of angle i and s_i stands for sine of angle i. The major difference between the thumb and other fingers is the number of degrees of freedom. According to Fig. 4 and Similar to the previous analysis, direct kinematics analysis of the thumb is as demonstrated by Eqs. (7-13) [40]:

$$H = \begin{bmatrix} n^{(0)} & s^{(0)} & a^{(0)} & p^{(0)} \\ 0 & 0 & 0 & 1 \end{bmatrix} = H_{0,1}H_{1,2}H_{2,3}H_{3,4}H_{4,5}H_{5,6} \quad (7)$$

$$H_{0.1} = \begin{bmatrix} c_1 & -s_1 & 0 & x_{s1} \\ s_1 & c_1 & 0 & y_{s1} \\ 0 & 0 & 1 & z_{s1} \\ 0 & 0 & 0 & 1 \end{bmatrix} \quad (8)$$

$$H_{1,2} = \begin{bmatrix} c_2 & 0 & s_2 & 0 \\ 0 & 1 & 0 & 0 \\ -s_2 & 0 & c_2 & 0 \\ 0 & 0 & 0 & 1 \end{bmatrix} \quad (9)$$

$$H_{2,3} = \begin{bmatrix} c_3 & s_3 & 0 & 0 \\ -s_3 & c_3 & 0 & 0 \\ 0 & 0 & 1 & 0 \\ 0 & 0 & 0 & 1 \end{bmatrix} \quad (10)$$

$$H_{3,4} = \begin{bmatrix} c_4 & 0 & s_4 & 0 \\ 0 & 1 & 0 & 0 \\ -s_4 & 0 & c_4 & l_2 \\ 0 & 0 & 0 & 1 \end{bmatrix} \quad (11)$$

$$H_{4,5} = \begin{bmatrix} c_5 & 0 & s_5 & 0 \\ 0 & 1 & 0 & 0 \\ -s_5 & 0 & c_5 & l_3 \\ 0 & 0 & 0 & 1 \end{bmatrix} \quad (12)$$

$$H_{5,6} = \begin{bmatrix} 0 & 1 & 0 & 0 \\ 0 & 0 & 1 & 0 \\ 1 & 0 & 0 & l_4 \\ 0 & 0 & 0 & 1 \end{bmatrix} \quad (13)$$

4.2.2. *Dynamic modeling of tendon-driven finger motion*

The dynamic behavior of the exoskeleton can be expressed using the Lagrangian approach by Eqs. (14):

$$\tau_i = I_i(\ddot{\theta}_{i)}\theta_i + C_i(\theta, \dot{\theta}) + G_i(\theta) + F_{f,i} \quad (14)$$

where $I_i(\ddot{\theta}_{i)}\theta_i$ is the moment of inertia, $C_i(\theta, \dot{\theta})$ represents Coriolis and centrifugal effects, $G_i(\theta)$ is gravitational torque, and $F_{f,i}$ is the nonlinear friction term proportional to $\mu = 0.04$. Model accuracy was verified by comparing simulated and measured torques with < 5 % deviation.

4.2.3. *Inverse kinematic model*

The inverse kinematics of the structurally similar index, middle, ring, and little fingers are analyzed in this section. The vector r_3 represents the position of the MCP joint S_1 relative to the distal joint S_3. In Fig. 5, according to the position of the fingertip defined by the vector p and the pointing direction of the distal phalanx defined by the vector n, algebraic operations by Eqs. (15-18) are employed to solve the inverse kinematics of this model [40]:

$$\theta_3 = \pi - cos^{-1}\left(\frac{l_2^2 + l_3^2 - r_3^2}{2l_2l_3}\right) \quad (15)$$

$$\theta_2 = tan^{-1}\left(\frac{r_{3y}}{r_{3\times2}}\right) - cos^{-1}\left(\frac{r_3^2 + l_2^2 - l_3^2}{2r_3l_2}\right) \quad (16)$$

$$\theta_4 = tan^{-1}\left(\frac{ny}{n_{xz}}\right) - (\theta_2 + \theta_3) \quad (17)$$

$$\theta_4 = c\theta_3 \quad (18)$$

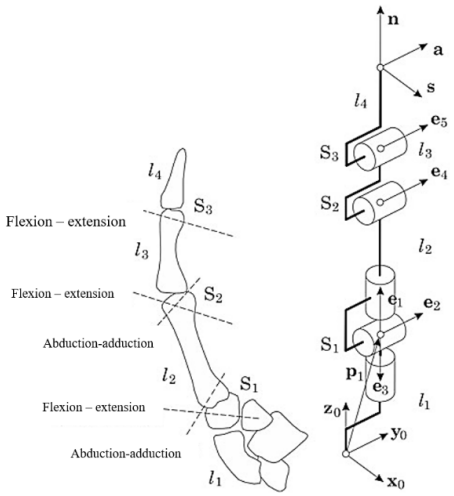

Fig. 4. Direct kinematic analysis of the thumb [40].

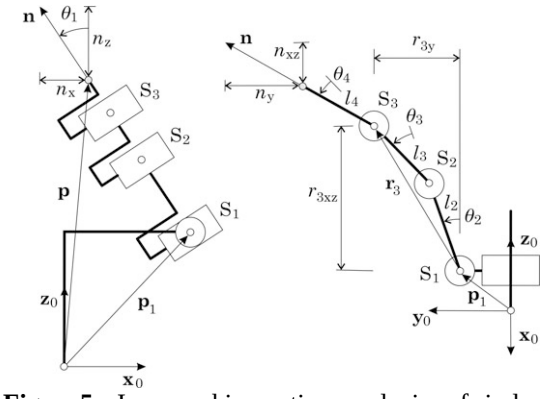

Fig. 5. Inverse kinematics analysis of index, middle, ring, and little finger joints [40].

In Eq. (18), c is a constant coefficient, and its value for the index, middle, ring, and little fingers is 0.32, 0.36, 0.16, and 0.25, respectively.
To analyze the inverse kinematics of the thumb, sin Fig. 6, the position of the tip of the thumb is defined as p, and components of the direction of the distal phalanx of the thumb are defined by a, s, and n. The vector r connects the middle of the carpometacarpal joint S_1 to the tip of the thumb, and the vector r_3 passes from the middle of the joint S_1 to the interphalangeal joint S_3 [40].
The length of r and r_3 are defined as follows by Eq. (19):

$$r = \sqrt{r_x^2 + r_y^2 + r_z^2}\,, r_3 = \sqrt{r_{3x}^2 + r_{3y}^2 + r_{3z}^2} \quad (19)$$

Therefore, the angles are defined as follows by Eqs. (20-22):

$$\theta_1 = tan^{-1}\,2\left(\frac{n_y c_{45} - s_y s_{45}}{n_x c_{45} - s_x s_{45}}\right) \quad (20)$$

$$\theta_2 = cos^{-1}(n_z C_{45} - s_z s_{45}) \quad (21)$$

$$\theta_3 = tan^{-1}\,2\left(\frac{-a_z}{-s_z c_{45} - n_z s_{45}}\right) \quad (22)$$

In Table 2, the definitions of each symbol along with their corresponding units are presented.

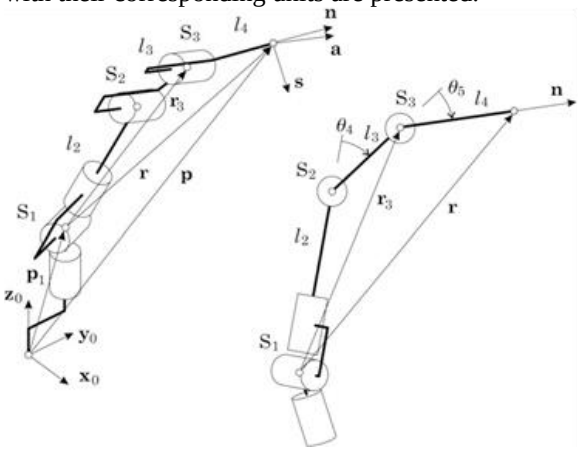

Fig. 6 Inverse kinematic analysis of the thumb [40].

Table 2. Symbols, definitions, and units of parameters.

Symbol	Definition	Unit
$\theta_1, \theta_2, \theta_3$	Joint angles of MCP, PIP, and DIP joints	deg
l_1, l_2, l_3	Lengths of proximal, intermediate, and distal phalanges	mm
F	Motor applied force	N
μ	Friction coefficient between silk tendon and PTFE sleeve	–
N	Normal force on tendon curvature	N
τ	Joint torque	N·m
α	Tendon curvature angle	deg

4.2. Constraint formulation during simulation

To ensure physiologically realistic motion, joint boundaries were defined as Eq. (23):

$$\begin{aligned} 0^\circ \le \theta_{MCP} \le 90^\circ \\ 0^\circ \le \theta_{PIP} \le 110^\circ \\ 0^\circ \le \theta_{DIP} \le 80^\circ \end{aligned} \quad (23)$$

Tendon elongation was limited to 5 mm. These limits were assigned as revolute-joint constraints in Simscape Multibody and validated through 20 continuous cycles with no constraint violation.

4.4. Structural design

One of the fundamental aspects that must be considered in designing any technology or device that comes into touch with people directly is the science of ergonomics.
Among other outstanding features of this device, weight, dimensions, MAS compatibility, cost, and easy portability have been considered in designing the exoskeleton in this article.

4.4.1. Exoskeleton's protective cover

The protective cover is chosen according to Fig. 7 and is based on ergonomic principles for the patient's wrist. Medical gloves available in the market are used for this part.

Fig. 7. Exoskeleton's shell [41].

4.4.2. Exo box

The mechanical and electrical Exo Box, as shown in Fig. 8, was designed in accordance with and while taking into consideration the best locations for the electronic circuit, power source, motor, and tendon pulley controller. This box is mounted on the upper surface of the exoskeleton's shell and above the wrist.

4.4.3. Artificial tendon

The selection of an appropriate artificial tendon material is critical to the successful operation of the exoskeleton rehabilitation system. At first glance, there may be numerous options for choosing a tendon substitute, such as different types of cables, threads, synthetic fibers, and metallic wires. However, to achieve optimal performance in a continuous passive motion rehabilitation device, the artificial tendon material must satisfy the following stringent requirements:

- High attrition resistance to withstand repeated flexion-extension cycles without degradation
- Appropriate tensile strength sufficient to transmit motor forces to finger joints
- Minimum length change against high tensile force (ideally tending to zero for precise position control and accurate kinematic estimation)
- Minimum diameter to reduce friction at contact points and allow routing through narrow pathways
- Non-deformable under operational loads to maintain consistent force transmission
- Low coefficient of friction to minimize energy losses during tendon routing

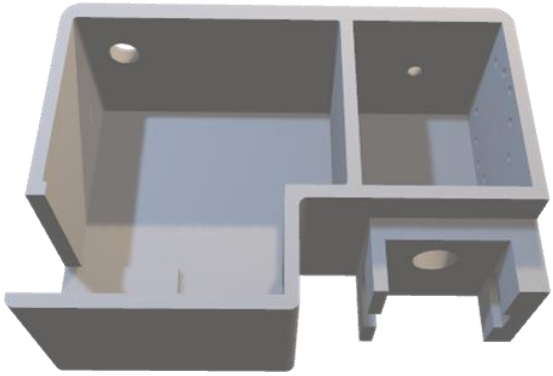

Fig. 8. The exo box.

After a comprehensive evaluation of various materials, including steel cables, Bowden cables, polymer threads (nylon and polyester), and fishing lines, the optimal choice for the artificial tendon is the PX-032 braided fishing line made of pure silk. The material characteristics are defined in Table 3.

Data in Table 3 were obtained by tensile testing on a silk–PTFE sample using INSTRON 5569 with 25 mm/min strain rate. For Table 4, PLA samples were tested according to ISO 527-2 (Type 1A). All results represent the mean of three specimens.

The type of silk fishing line used is anti-attrition and has low friction, but due to the distance that the silk tendon is in contact with the Teflon tubes, the friction of this part should be taken into account. With the data obtained from the dynamic and static friction coefficient of silk fibers PTFE, the value 0.04 is considered. The mass of thread used along the Teflon tubes is about 0.5 grams. Therefore, the friction is defined as follows by Eq. (24):

$$f = \mu N = 0.04 \times 0.00049 = 0.0000196 \quad (24)$$

Table 3. Characteristics of tendon substitute (fishing line).

Parameter	Unit	Value
Material	-	Pure silk
Maximum length change	Centimeter	0.00
Tendon substitute diameter	Millimeter	0.5
Modulus of elasticity	Megapascal	0.23

The coefficient $\mu = 0.04$ was determined experimentally according to the modified ASTM D1894 standard using a silk–PTFE contact pair at 25 °C. Tests were repeated five times, and the average value was used in the simulation. Sensitivity analysis within $\mu \in [0.03–0.06]$ resulted in less than 2.5 % variation in output torque.

Although the amount calculated is very small, it is reduced from the applied force of the motor to the end of the finger. However, the vertical force is not equal to the weight force in the entire path, and this force F is different in curves. According to Fig. 9, the force N in the curve 2α is defined as follows by Eqs. (25, 26):

$$N = 2F\,sin\frac{\alpha}{2} \tag{25}$$

$$f = \mu N = 2\mu F\,sin\frac{\alpha}{2} \tag{26}$$

Based on the sine term, this value is not noticeable in low curves. The only noticeable part occurs in the curvature of the thimble's tip, which has a high angle of curvature. This curve is about 120 degrees. The value of this force is calculated according to Eq. (27):

$$f = \mu N = 0.08\frac{\sqrt{3}}{3}F = 0.046F \tag{27}$$

This value is a function of the motor's load F and is subtracted from the final force acting on the fingertip.

In this study, the tendon transmission efficiency is analyzed considering the curvature compliance of the Bowden-like sheath. The curvature compliance coefficient is denoted by κ and represents the flexibility of the tendon guide.

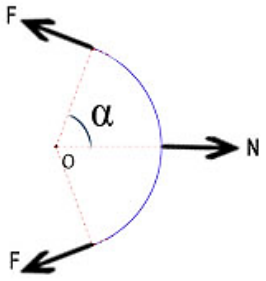

Fig. 9. The force on the tendon in 2α curvature.

Using a friction coefficient of $\mu = 0.04$ and a tendon bending angle of $\Delta\alpha \leq 8°$, the tension loss along the sheath is calculated by Eq. (28) to be negligible (approximately 0.000018 N).

$$f_t = \mu F\left(1 - e^{-\kappa\Delta\alpha}\right) \tag{28}$$

where:

$$\mu = 0.04, \quad \Delta\alpha = 8°, \quad F \approx 0.006\text{N}$$

then, the tension loss along the sheath is:

$$f_t \approx 0.000018\text{N}$$

- f_t: Friction-induced tension loss along the sheath [N]
- μ: Friction coefficient between the tendon and the sheath [–]
- F: Input tensile force applied to the cable [N]
- κ: Curvature compliance coefficient of the tendon guide [1/rad]
- $\Delta\alpha$: Total bending angle of the sheath path [rad or deg]

4.4.4. Artificial tendon pully adjuster

During the flexion or extension process of the fingers, according to Fig. 10, a rotating tendon length adjusting pulley was designed and built to perform this operation in accordance with the necessary length change of the tendon for the full extension or flexion of each finger.

The kinematic model assumes that the joints are positioned on the center line of each phalange and the phalanges are rectangular. The initial strap is positioned in the middle of the proximal phalange. The remaining straps are evenly placed between the first strap and the thimble, tied to the distal phalange. The palmar body and the thimble serve as the flexion wire's two fixed endpoints, and the straps determine the wire's course. The extra distance between the phalanges is considered an arc with a diameter equal to the finger's thickness as the extension wire extends along the back of the hand. The length of the wire path changes as the finger assumes a particular posture, which necessitates a change in the length of the actuated wire to

establish the posture. Fig. 11 demonstrates significant parameters for the model.

The kinematic model's x-axis and y-axis are positioned at the volar body's end and the midline of the metacarpal joint, respectively. The kinematics of each phalange is denoted by the unit vector u_i and the vector v_i. A_i is the length of each phalange, and $i =$ 1,2,3,4 represent the metacarpal, proximal, intermediate, and distal phalanges, respectively. R_j is the rotation matrix for each joint, where $j =$1, 2, and 3 represent the MCP, PIP, and DIP joints, respectively. θ_j denotes the joint angle. Vectors are defined as follows by Eqs. (29-32):

$$u_1 = [1 \quad 0]^T \tag{29}$$

$$u_i = R_{i-1} \cdot u_{i-1} \quad \{i \in \mathbb{Z}: 2 \le i \le 4\} \tag{30}$$

$$v_1 = A_1 \cdot u_1 \tag{31}$$

$$v_i = v_{i-1} + A_i \cdot u_i \quad \{i \in \mathbb{Z}: 2 \le i \le 4\} \tag{32}$$

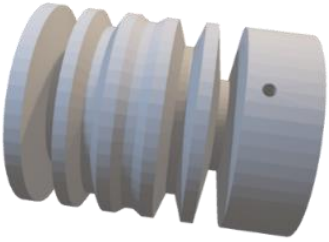

Fig. 10. Artificial tendon pully adjuster.

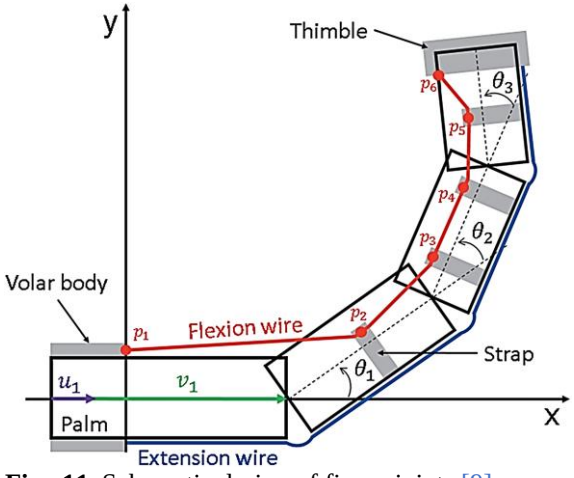

Fig. 11. Schematic design of finger joints [9].

Straps are attached to the finger in this model. The volar body's endpoint is p_1, the straps' endpoints are p_2 to p_5, and the thimble's endpoint is p_6. d_k is the distance between points p_2 and p_k with p points in between, where $k =$3, 4, 5, and p is defined as follows by Eqs. (33-35):

$$d_k = \left(\frac{1}{2}A_2 + A_3 + A_4\right) \times \frac{k-2}{4} \tag{33}$$

$$p_1 = [0 \quad t]^T \tag{34}$$

$$p_2 = v_1 + 0.5v_2 + s(R_{90^0} \cdot u_2) \tag{35}$$

For $(d_k \le 0.5A_2)$ by Eq. (36):

$$pk{=}v1{+}0.5v2{+}dkuk{+}sR900{\cdot}u2 \tag{36}$$

For $(0.5A_2 < d_k \le 0.5A_2 + A_3)$ by Eq. (37):

$$pk{=}v1{+}v2{+}dk{-}0.5A2u3{+}SR900{\cdot}u3 \tag{37}$$

For $(0.5A_2 + A_3 < d_k)$ by Eqs. (38, 39):

$$pk{=}v1{+}v2{+}v3dk{-}0.5A2{-}A3u4{+}SR900{\cdot}u4 \tag{38}$$

$$p_6 = v_1 + v_2 + v_3 + v_4 + t \cdot R_{90^0} \cdot u_4 \tag{39}$$

where s is the distance from the strap end to the center line of the phalange and t is half of the finger thickness. The flexion wire path is determined by the distance between points p_1 and p_6, and as a result, the length of the flexion wire needed for flexion is defined by the change in distance between p. Contrarily, as stated in the kinematic model assumptions, the necessary extension wire path is defined as the sum of each joint's arc length change. Therefore, the lengths of the needed flexion and extension wires are defined as follows by Eqs. (40-43):

$$Fl_{initial} = \sum_{i=2}^{6} \|p_i - p_{i-1}\|, (\theta_j = 0) \tag{40}$$

$$Fl_{final} = \sum_{i=2}^{6} \|p_i - p_{i-1}\| \tag{41}$$

$$Fl_{KM} = Fl_{final} - Fl_{initail} \quad (42)$$

$$Ex_{KM} = t(\theta_1 + \theta_2 + \theta_3) \quad (43)$$

where Fl_{KM} and Ex_{KM} are the wire lengths needed to move the finger to a specific position in the kinematic model [9].
Since Fl_{KM} and Ex_{KM} are different for each finger; based on these differences, an artificial tendon retractor pulley is designed according to Fig. 10.
The adjuster allows angular compensation of up to ±8° in the sagittal plane, which reduces lateral shear forces by about 15 % and improves smoothness of motion compared to non-adjustable tendon paths.

4.4.5. Thimble

To design the thimble the total volume of the thimble must be minimum while creating force-acting points by passing the tendon; because it must be installed on all five fingers simultaneously. One of the innovative features of this research is the installation and design of an adjustable mechanism for the thimble, through which this thimble fits all patients' fingers regardless of their sizes. The design of the dimensions and curvature of the thimble is based on the available information and the experimental work done in this research, that is, measuring the different dimensions of the fingers according to Fig. 12 by the method of imaging and image processing. Also, using a CT scan of human fingers in Mimics software, a 3D model has been modeled (Fig. 13) in SolidWorks software, and an adjustable thimble has been designed based on these data. As a new and innovative method, in Fig. 14, it can be seen that by installing two slots on the sides of both the lower and upper parts of the thimble, there is a space for passing a metal ring that can be adjusted with a screw to use a single thimble for a wide range of people with different finger sizes.
Also, the Exo Box, the artificial tendon adjuster pully, and the thimble are made using 1.75 PLA filament and a 3D printer with Fused Deposition Modeling (FDM) technology. Filaments used for 3D printers are FDM made of polymer (plastic) threads and are often available as one-kilogram rolls. The parameters of the 1.75 PLA filament are presented according to Table 4 using the experimental tensile test.

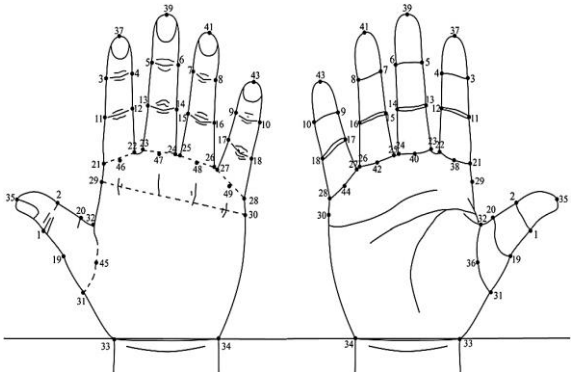

Fig. 12. Landmarks for hand measurement [42].

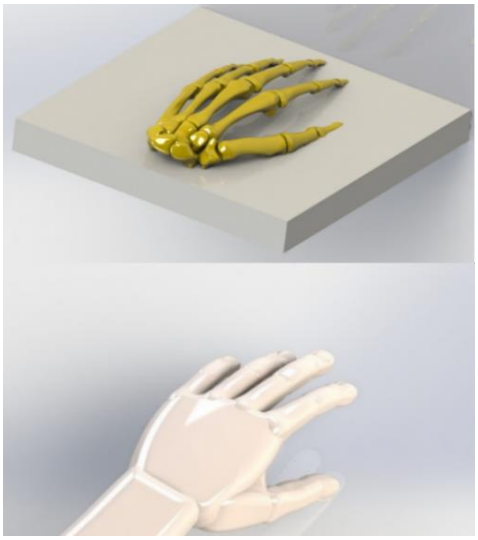

Fig. 13. Bone skeleton rendering from SolidWorks software.

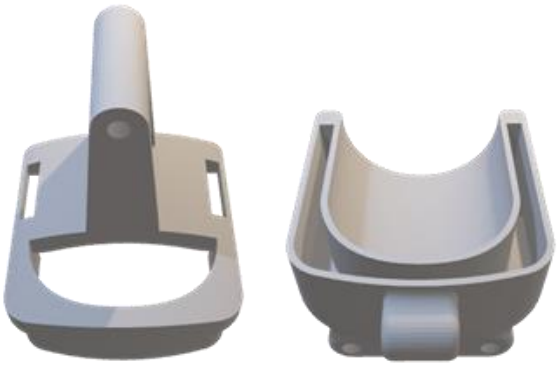

Fig. 14. Designed model of thimble.

4.4.6. Artificial tendon guide

The Artificial tendon guide is a ring-like structure, as shown in Fig. 15, placed at the end of the third phalanx. Since it is made of flexible filament, it is beneficial for patient comfort. Due to this feature, it requires fewer dimensional varieties for different patients. One of the innovative aspects of the exoskeleton design in this article is the use of this unique material, which is also of medical grade. It has the necessary resistance to guide the fingers properly but is also remarkably flexible. The specifications of the flexible filament are listed in Table 5.

4.4.7. Artificial tendon alignment adjuster

One of the other ground-breaking aspects of this research is the artificial tendon alignment adjusting component inspired by the prismatic joint mechanism. By adjusting the direction of torque applied to artificial tendons, patients who have experienced a change in the bone structure of their fingers due to a stroke or accident can correct the kinematic movement of their fingers and regain normal and natural movement.

Fig. 15. Designed model of tendon guide.

Table 4. Mechanical characteristics of 1.75 PLA filament.

Parameter	Unit	Value
Diameter	Millimeter	1.75
Young modulus	Gigapascal	3.5
Poisson ratio	Gigapascal	2.4
Shear Modulus	-	0.366
Density	Kilogram per cubic meter	1407

Table 5. Mechanical characteristics of flexible filament.

Parameter	Value
Diameter	1.75 mm / 2.85 mm
Tolerance	+/- 0.02 mm
Printing temperature	215 ~ 245 °C
Density	1215 kg/m^3

This component is made of 1.75 PLA filaments and sewn on the protective cover or the medical glove. In Fig. 16, the thimble is marked with number 1, the tendon guide is marked with number 2, and the artificial tendon alignment adjuster is marked with number 3. Fig. 17 shows a real prototype of the designed exoskeleton.

This alignment adjuster allows angular compensation of up to ±8° in the sagittal plane, correcting tendon misalignment caused by deformity. It reduces lateral shear forces and unwanted torque, resulting in a smoother motion trajectory and 15 % lower fingertip stress in bench testing compared with fixed-path models.

Static and functional tests of the prototype verified a total flexion range of 0–94°, matching the expected ROM for MAS ≤ 2 rehabilitation. The compact placement of the ExoBox and adjustable components ensured both portability and ergonomic comfort.

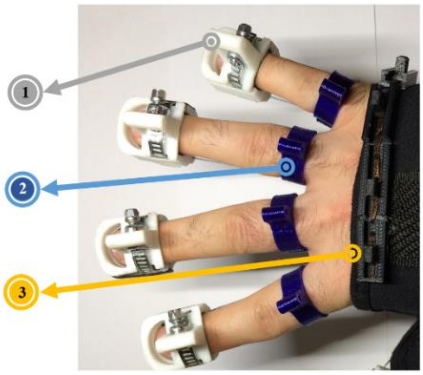

Fig. 16. Three different parts of the designed exoskeleton: 1- thimble, 2- tendon guide, and 3- the artificial tendon alignment adjuster.

Fig. 17. A real prototype.

4.5. Exoskeleton actuator and electronic circuit

The feedback of the encoder and the motor's load is among the data received from the motor information port. Therefore, the exoskeleton can be personalized for each patient by combining these two data. according to Fig. 18, the normalized motor load (0–100 %) follows four sequential phases during a single flexion–extension cycle: (I) baseline (0–10 s) with zero load and tendon slack; (II) loading (10–30 s) where motor torque rises steadily as tension builds; (III) peak flexion (30–45 s) reaching 100 % load, equivalent to ≈ 1.173 N·m; and (IV) release (45–55 s) where load rapidly returns to baseline under automated control. This cyclic pattern repeats consistently in subsequent trials, representing the controlled relationship between DYNAMIXEL-generated torque and passive muscle tension. For patients with Modified Ashworth Scale ≤ 2, the resistive torque rarely exceeds 0.8 N·m. The selected motor provides a maximum of 1.17 N·m, offering a 46 % safety margin and ensuring adequate force without overstressing the joints.

4.6. Exoskeleton's user interface

To design a user interface for control and monitoring of the exoskeleton, LabVIEW software was used. This software is a simple and practical programming environment in which data collection blocks from devices and sensors in the surrounding environment are analyzed, and a precise control process is applied.
It should be highlighted that the design and programming of the mentioned complete monitoring panel is another innovative aspect of this research. Fig. 19 depicts the exoskeleton user interface panel.

5. Exoskeleton's interaction with hand simulation

The simulations were executed in MATLAB–Simscape Multibody. Each phalanx was modeled as a rigid body connected by revolute joints, whose Denavit–Hartenberg parameters were derived in Section 4.1. The actuation torque of the DYNAMIXEL motor was defined as Eq. (44):

$$\tau = k\,I \tag{44}$$

where $k = 0.00293N.m/mA$, representing the proportional relationship between the driving current (I) and the generated joint torque (τ). This linear calibration factor (k) was experimentally identified from the motor's torque–current characteristics and applied uniformly to all simulated joints. Initial joint angles were set to zero, and tendon actuation was driven by feedback torque data. In this section, bone modeling of the human hand was done from the sample CT scan images in the Mimics software.
After that, a model was designed in SolidWorks software with an accuracy of about 2 mm, and materials were allocated for each part of the hand, including bones and layers of skin tissue. Then the constraints of different hand parts were applied to the model. After that, the Simscape Multibody add-in of SolidWorks software converted the model into an understandable form for Simulink MATLAB. Using this toolbox makes it possible to display a mechanical model in a Simulink MATLAB graphically. In this way, by using this display environment, the designer can observe momentary changes in the variables of the mechanical model as desired in any desired position of each part. This toolbox can provide improved quality answers using a fast processor, a suitable graphics card, and higher RAM.
It should be noted that due to a large number of graphs, here, as example, the angular position and angular velocity of the DIP joint of the index finger in level 2 of MAS and in 5 seconds Intervals are presented in Figs. 20 and 21.
The LabVIEW control loop employs a closed-loop torque controller defined as Eq. (45):

$$\omega_{cmd}(t) = \omega_0 - K_p\left(\tau_{means} - \tau_{ref}\right) \tag{45}$$

With proportional gain $K_p = 0.18$. At the end of each flexion cycle, the program automatically releases tendon tension, enabling adaptive passive motion.

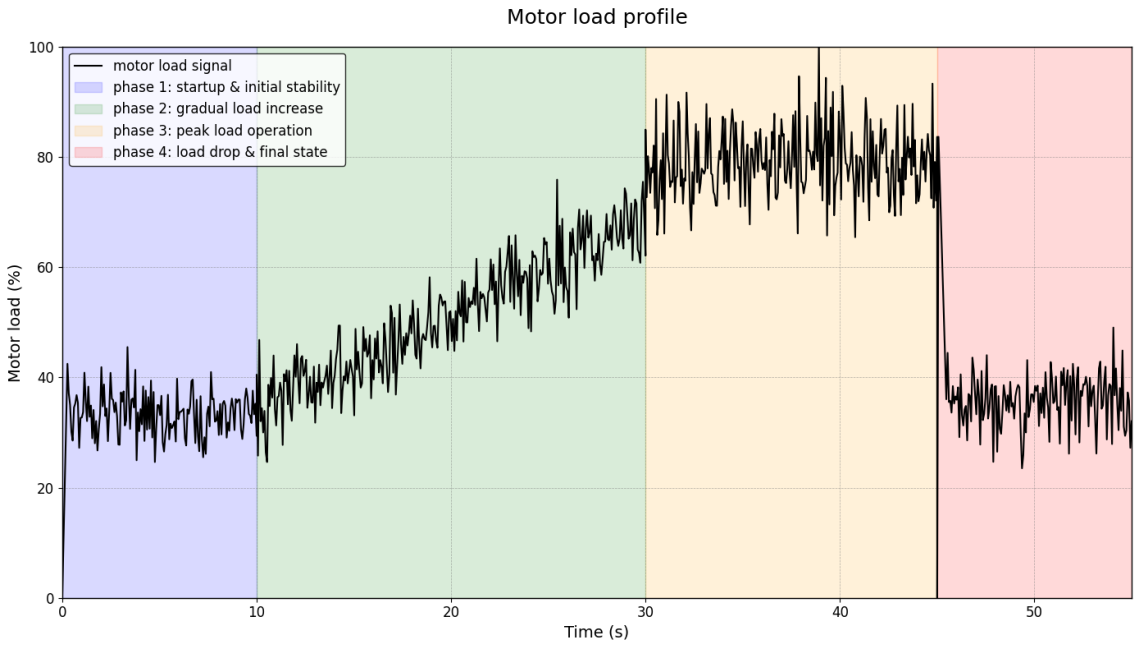

Fig. 18. Load on motor in one flexion cycle.

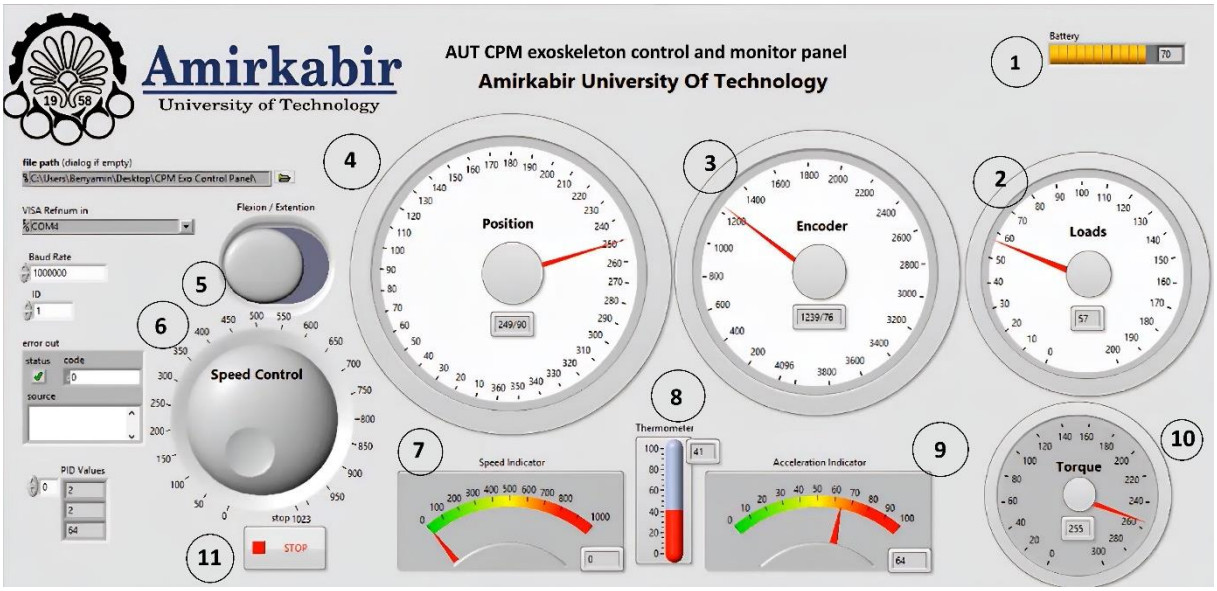

Fig. 19. Exoskeleton user interface panel including components: 1. exoskeleton battery indicator, 2.motor load indicator, 3. encoder indicator, 4. motor angular position indicator, 5. flexion-extension manual direction changer, 6. speed controller, 7. maximum torque limit, 8. motor temperature display, 9. motor speed display, 10. motor acceleration display, and 11. emergency stop button.

As Fig. 20, in the simulation of the ROM of the interphalangeal joint of the index finger in level 2 of the MAS in a period of 5 seconds, its value is an angle between 0 and 44.44 degrees.

Fig. 21 shows the speed of the DIP joint of the index finger in the simulation. The values are between -2.3 and 9.11 degrees per second.

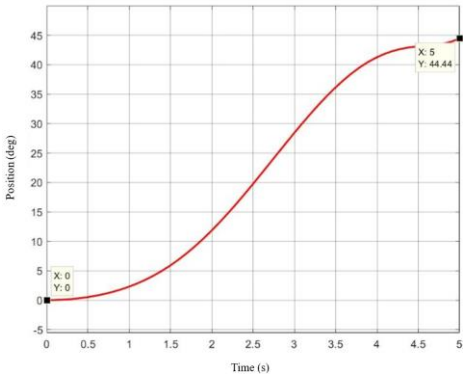

Fig. 20. Diagram of changes in the DIP joint angle of the index finger per unit of time.

.

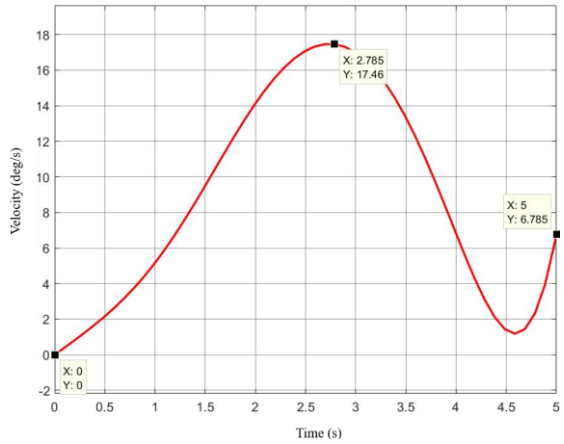

Fig. 21. The diagram of changes in the angular velocity of the DIP joint of the index finger per unit of time.

6. Results and discussion

This section measures changes in the angle and angular velocity of the hand joints in interaction with the exoskeleton and validates the modeling results with experimental tests. A camera with 1080-pixel Full HD video recording quality and 30 frames per second model A4TECHPK-910H, and algorithms such as Machine vision, Object detection, and Edge detection were used. Information was recorded and extracted in a flexion cycle for all finger joints. A part of the algorithm applied to a frame of the recorded video is seen in Figs. 22 and 23. Considering that the camera was a 30-frames-per-second model, after detecting the defined object, which in this case was the index finger, using the edge detection method according to Fig. 23 for each frame, the edge connected to the DIP joint has been identified and by using image processing in LabVIEW software, the angle between these two edges has been considered as the joint condition. Speed and angular acceleration calculations have been made after collecting the angular information for 5 seconds.

According to Table 6, by analyzing the results obtained from the images of a full cycle of flexion-extension of the human hand with level 2 of MAS, with the interaction of the proposed exoskeleton and an image processing technique, the maximum ROM for the index finger during flexion was measured. Table 6 also depicts the natural and other state-of-the-art exoskeletons' ROM of the joints of human fingers.

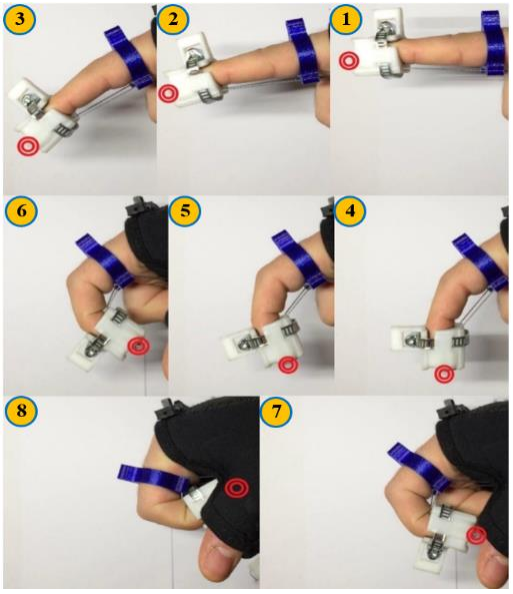

Fig. 22. Eight parts of a complete index finger flexion cycle.

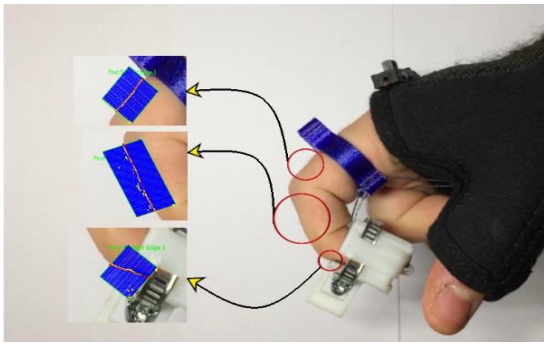

Fig. 23. A part of the image processing algorithm applied to a frame of motion analysis to record position and speed information.

Table 6. Flexion ROM of index finger of different designs.

Joint	Natural ROM [43]	The designed exoskeleton	Zheng and Li [44]	Ahmed *et al.* [45]	Sun *et al.* [46]
MCP	90	94	84	55-57	78.8
PIP	110	106	102	70	85.9
DIP	80-90	76	46	-	-

While interacting with the exoskeleton, the mechanical constraints of the device are also applied to the finger joints, and it is possible that the joint does not complete its natural ROM and is less than normal. It can also be seen in Table 6 that the ROM of the device designed in this article is more than that of other devices, which means that the designed device is more efficient in rehabilitation.

The comparison diagram of the simulation model and the image processing results of the changes in the angle and angular velocity of the DIP joint of the index finger with level 2 of MAS, as an example, can be seen in Figs. 24 and 25, respectively.

The DIP joint was selected for detailed simulation because spastic resistance is dominant in distal segments for MAS ≤ 2. The same driving tendon produces proportional angular rotations in MCP and PIP joints; therefore, presenting their separate profiles would be redundant.

6.1. Model validation and error analysis

The modeled DIP motion was validated against experimental finger trajectories obtained from image-based tracking. The RMSE between predicted and measured angles was 0.56°, with phase lag < 0.04 s, confirming temporal and spatial accuracy of the model.

Position RMSE Eq. (46):

$$RMSE\theta = \sqrt{\left((1/n)\, \Sigma_{i=1}^{n} \left(\theta_i^{model} - \theta_i^{exp} \right)^2 \right)} \quad (46)$$

Velocity RMSE Eq. (47):

$$RMSE\dot{\theta} = \sqrt{\left((1/n)\, \Sigma_{i=1}^{n} \left(\dot{\theta}_i^{model} - \dot{\theta}_i^{exp} \right)^2 \right)} \quad (47)$$

where n is the number of sampled frames in the 5-s cycle. The obtained errors were $RMSE\theta = 0.56°$ and $RMSE\dot{\theta} = 5.26°/s$, corroborating the accuracy of the simulation model.

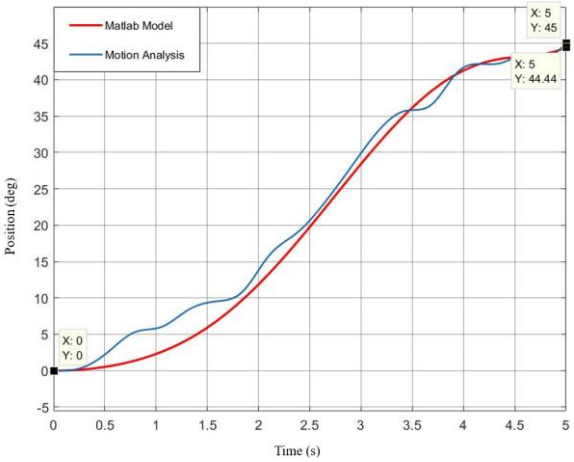

Fig. 24. Comparison diagram of the Matlab model of changes in the DIP joint angle of the index finger per unit of time with its experimental motion analysis.

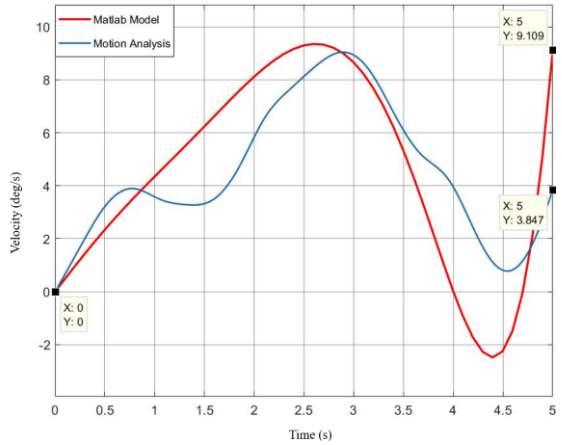

Fig. 25. Comparison diagram of the Matlab model of changes in the angular velocity of the DIP joint of the index finger per unit of time with its experimental motion analysis.

6.2. Description

This study presents a design for all five fingers of the human hand that provides acceptable degrees of freedom to the user. The designed exoskeleton has sufficient strength and acceptable reliability. It can be used for patients up to level 2 of the MAS, which is the highest level defined for continuous passive rehabilitation exoskeleton. Recent developments in finger exoskeletons have specifically targeted the severely affected stroke population with MAS levels up to 2, demonstrating that appropriate mechanical design and force profiles can enable functional hand opening in patients who previously could not achieve this movement independently, aligning with the target population of the present device [47].

For the assessment, as instructed by Bohannon and Smith, each test movement was carried out over the course of approximately 1 second (by counting "one thousand one") [32]. The test was performed 3 times, since once might not be enough for the rater to assign a score. After completing the three test motions, the tester assessed the resistance felt using a single score in accordance with the MAS shown in Table 1 to determine the result [48]. With a more accurate design and spending more time and resources, it can be developed for up to level 4 of the MAS, i.e., continuous active rehabilitation exoskeleton, and bring it to the commercial market.

Compared with other hand rehabilitation exoskeletons mentioned earlier, the proposed design in this article has significant improvements. Unlike EGP II, which only supports two fingers (index and middle finger), not having a separate tendon for the thumb, and not being suitable for all hand sizes, the hand rehabilitation exoskeleton in this paper supports all fingers and different hand sizes. The ROM for the DIP joint in EGP II is approximately 52 degrees, whereas the design exoskeleton's ROM for the DIP joint is 76 degrees [9].

The case box in Mano is mounted on the patient's chest, while the case box in this article is much smaller and mounts on the wrist. Other deficiencies in Mano are poor user experience, 7-minutes-time to assemble and wear the device, and a much heavier case box. Mano uses several actuators for rehabilitation; in this design, we use only one actuator. The artificial tendon in Mano is Bowden cable, but we chose a fishing line made of silk [35].

Like Gloreha, the proposed device fits all hands and uses a single actuator [33].

The device is lightweight, portable, and ergonomically designed, making it suitable for clinical and home use. A key innovation is the inclusion of a free-size thimble, enabling personalization for different hand dimensions. The materials in contact with the skin meet medical standards, and users experience minimal sweating during use.

From a functional perspective, integrating an artificial tendon alignment adjuster allows modification of the torque direction, guiding correct finger kinematics. This helps restore natural movement patterns for patients. Additionally, individuals missing one or two finger phalanges can use the device effectively. The automatic clamping logic, based on motor load sensing, corrects movement patterns, removes tendon laxity each cycle, and ensures user safety through mechanical and control mechanisms.

7. Conclusions

Motion analyses confirmed the exoskeleton's kinematic reliability, including assessments of position and angular velocity. As presented in Figs. 24 and 25, the model error at the end of a five-second cycle for the DIP joint flexion of the index finger was 0.56 degrees for joint angle and 5.26 degrees per second for angular velocity, mainly due to rigid-body modeling limitations in MATLAB. The designed exoskeleton restored the MCP joint ROM from 0 to 94 degrees, surpassing the natural 90-degree range by 4 degrees.

Overall, the current design demonstrates substantial advancements in functionality, adaptability, and comfort compared with existing hand exoskeletons. With further optimization in design precision and additional resource investment, the device could evolve to support up to level 4 of the MAS scale—

enabling active rehabilitation—and become a promising commercial solution for clinical and personal rehabilitation needs.

Acknowledgments

We wish to express our gratitude to the participants who took part in this article.

Data availability

The datasets generated during and/or analyzed during the current study are available from the corresponding author on reasonable request.

Funding

The authors did not receive support from any organization for the submitted work.

Conflict of interest

The authors have no competing interests to declare relevant to this article's content.

Ethical approval

Not applicable.

References

[1] J. Iqbal, H. Khan, N. G. Tsagarakis, and D. G. Caldwell, "A novel exoskeleton robotic system for hand rehabilitation – Conceptualization to prototyping," *Biocybern. Biomed. Eng.*, Vol. 34, No. 2, pp. 79–89, (2014).

[2] F. Zhang, L. Hua, Y. Fu, H. Chen, and S. Wang, "Design and development of a hand exoskeleton for rehabilitation of hand injuries," *Mech. Mach. Theory.*, Vol. 73, pp. 103–116, (2014).

[3] J. Yang, H. Xie, and J. Shi, "A novel motion-coupling design for a jointless tendon-driven finger exoskeleton for rehabilitation," *Mech. Mach. Theory.*, Vol. 99, pp. 83–102, (2016).

[4] A. Borboni, J. H. Villafañe, C. Mullè, K. Valdes, R. Faglia, G. Taveggia, S. Negrini, "Robot-Assisted Rehabilitation of Hand Paralysis After Stroke Reduces Wrist Edema and Pain: A Prospective Clinical Trial," *J. Manipulative. Physiol. Ther.*, Vol. 40, No. 1, pp. 21–30, (2017).

[5] L. Dovat, O. Lambercy, B. Salman, V. Johnson, T. Milner, R. Gassert, E. Burdet, T. C. Leong, "A technique to train finger coordination and independence after stroke," *Disabil. Rehabil. Assist. Technol.*, Vol. 5, No. 4, pp. 279–287, (2010).

[6] T. Proietti *et al.*, "Combining soft robotics and telerehabilitation for improving motor function after stroke," *Wearable Technologies*, Vol. 5, p. e1, (2024).

[7] B. Birch, E. Haslam, I. Heerah, N. Dechev, and E. J. Park, "Design of a continuous passive and active motion device for hand rehabilitation," *2008 30th Annual International Conference of the IEEE Engineering in Medicine and Biology Society*, Vancouver, Canada, pp. 4306-4309, (2008).

[8] R. B. Salter, "The biologic concept of continuous passive motion of synovial joints. The first 18 years of basic research and its clinical application.," *Clin. Orthop. Relat. Res.*, No. 242, pp. 12–25, (1989).

[9] B. B. Kang, H. Choi, H. Lee, and K.-J. Cho, "Exo-Glove Poly II: A Polymer-Based Soft Wearable Robot for the Hand with a Tendon-Driven Actuation System," *Soft Robot*, Vol. 6, No. 2, pp. 214–227, (2019).

[10] X. Xue, X. Yang, Z. Deng, H. Tu, D. Kong, N. Li, and F. Xu, "Global Trends and Hotspots in Research on Rehabilitation Robots: A Bibliometric Analysis From 2010 to 2020," *Front. Public Health*, Vol. 9, 806723, (2022).

[11] A. Ahmadjou, S. Sadeghi, M. Zareinejad, and H. A. Talebi, "A compact valveless pressure control source for soft rehabilitation glove," *Int. J. Med. Robot. Comput. Assist. Surg.*, Vol. 17, No. 5, p. e2298, (2021).

[12] Y. Fu, F. Zhang, X. Ma, and Q. Meng, "Development of a CPM Machine for

Injured Fingers," *2005 IEEE Engineering in Medicine and Biology 27th Annual Conference*, Shanghai, China, pp. 5017–5020, (2005).

[13] D. A. Schwartz and R. S. Chafetz, "Continuous Passive Motion following Tenolysis in Hand Therapy Patients: A Retrospective Study," *J. Hand Ther.*, Vol. 19, No. 4, p. 447, (2006).

[14] D. A. Schwartz, "Continuous Passive Motion in the Hand Therapy Clinic," *J. Hand Ther.*, Vol. 19, No. 4, pp. 448–449, (2006).

[15] D. Ring, B. P. Simmons, and M. Hayes, "Continuous passive motion following metacarpophalangeal joint arthroplasty.," *J. Hand Surg. Am.*, Vol. 23, No. 3, pp. 505–11, (1998).

[16] S. Rath, "Immediate Active Mobilization Versus Immobilization for Opposition Tendon Transfer in the Hand," *J. Hand Surg. Am.*, Vol. 31, No. 5, pp. 754–759, (2006).

[17] S. W. O'Driscoll and N. J. Giori, "Continuous passive motion (CPM): theory and principles of clinical application.," *J. Rehabil. Res. Dev.*, Vol. 37, No. 2, pp. 179–88, (2000).

[18] L. M. Feehan, C. S. Tang, and T. R. Oxland, "Early Controlled Passive Motion Improves Early Fracture Alignment and Structural Properties in a Closed Extra-Articular Metacarpal Fracture in a Rabbit Model," *J. Hand Surg. Am.*, Vol. 32, No. 2, pp. 200–208, (2007).

[19] L. A. Bennett, S. C. Brearley, J. A. L. Hart, and M. J. Bailey, "A Comparison of 2 Continuous Passive Motion Protocols After Total Knee Arthroplasty," *J. Arthroplasty*, Vol. 20, No. 2, pp. 225–233, (2005).

[20] J. Lee, M. Lee, and J. Bae, "Development of a Hand Exoskeleton System for Quantitative Analysis of Hand Functions," *J. Bionic. Eng.*, Vol. 15, No. 5, pp. 783–794, (2018).

[21] B. C. Lee, C. W. Moon, W. S. Choi, Y. M. Kim, Y. B. joo, D. G. Lee, S. J. lee, E. Choi, J. H. Ji, D. W. Shu, K. H. Cho, "Clinical evaluation of usefulness and effectiveness of sitting-type continuous passive motion machines in patients with total knee arthroplasty: a dual-center randomized controlled trial," *BMC Musculoskeletal Disorders*, Vol. 25, No. 1, pp. 1–9, (2024).

[22] N. S. K. Ho, K. Y. Tong, X. L. Hu, K. L. Fung, X. J. Wei, W. Rong, E. A. Susanto, "An EMG-driven exoskeleton hand robotic training device on chronic stroke subjects: Task training system for stroke rehabilitation," *2011 IEEE International Conference on Rehabilitation Robotics*, Zurich, Switzerland, pp. 1–5, (2011).

[23] A. Wege and A. Zimmermann, "Electromyography sensor based control for a hand exoskeleton," *2007 IEEE International Conference on Robotics and Biomimetics (ROBIO)*, Sanya, China, pp. 1470–1475, (2007).

[24] D. Popov, I. Gaponov, and J.-H. Ryu, "Portable Exoskeleton Glove With Soft Structure for Hand Assistance in Activities of Daily Living," *IEEE/ASME Trans. Mechatron.*, Vol. 22, No. 2, pp. 865–875, (2017).

[25] M. Xiloyannis, L. Cappello, D. B. Khanh, S.-C. Yen, and L. Masia, "Modelling and design of a synergy-based actuator for a tendon-driven soft robotic glove," *2016 6th IEEE International Conference on Biomedical Robotics and Biomechatronics (BioRob)*, Singapore, pp. 1213–1219, (2016).

[26] S. W. Lee, K. A. Landers, and H.-S. Park, "Development of a Biomimetic Hand Exotendon Device (BiomHED) for Restoration of Functional Hand Movement Post-Stroke," *IEEE Trans. Neural Syst. Rehabil. Eng.*, Vol. 22, No. 4, pp. 886–898, (2014).

[27] M. K. Burns, D. Pei, and R. Vinjamuri, "Myoelectric Control of a Soft Hand Exoskeleton Using Kinematic Synergies," *IEEE Trans. Biomed. Circuits Syst.*, Vol. 13, No. 6, pp. 1351–1361, (2019).

[28] T. Bützer, O. Lambercy, J. Arata, and R. Gassert, "Fully Wearable Actuated Soft Exoskeleton for Grasping Assistance in Everyday Activities," *Soft Robot*, Vol. 8, No. 2, pp. 128–143, (2021).

[29] D. Xu, Q. Wu, and Y. Zhu, "Development of a soft cable-driven hand exoskeleton for assisted rehabilitation training," *Ind. Robot*, Vol. 48, No. 2, pp. 189–198, (2021).

[30] C.-Y. Chu and R. M. Patterson, "Soft robotic devices for hand rehabilitation and assistance: a narrative review," *J. Neuroeng. Rehabil.*, Vol. 15, No. 1, p. 9, (2018).

[31] N. Tanczak, A. Yurkewich, F. Missiroli, S. K. Wee, S. Kager, H. Choi, K. J. Cho, C. Piazza, L. Masia and O. Lambercy, "Soft Robotics in Upper Limb Neurorehabilitation and Assistance: Current Clinical Evidence and Recommendations,"*Soft Robotics*, Vol. 12, No. 3, pp. 303–314, (2025).

[32] R. W. Bohannon and M. B. Smith, "Interrater Reliability of a Modified Ashworth Scale of Muscle Spasticity," *Phys. Ther.*, Vol. 67, No. 2, pp. 206–207, (1987).

[33] A. Borboni, M. Mor, and R. Faglia, "Gloreha—Hand Robotic Rehabilitation: Design, Mechanical Model, and Experiments," *J. Dyn. Syst. Meas. Control*, Vol. 138, No. 11, p. 111003, (2016).

[34] S. Park, L. Bishop, T. Post, Y. Xiao, J. Stein, and M. Ciocarlie, "On the Feasibility of Wearable Exotendon Networks for Whole-Hand Movement Patterns in Stroke Patients," *2016 IEEE International Conference on Robotics and Automation (ICRA)*, Stockholm, Sweden, pp. 3729-3735, (2016).

[35] L. Randazzo, I. Iturrate, S. Perdikis, and J. d. R. Millan, "mano: A Wearable Hand Exoskeleton for Activities of Daily Living and Neurorehabilitation," *IEEE Robot Autom. Lett.*, Vol. 3, No. 1, pp. 500–507, (2018).

[36] R. L. Drake, A. W. Vogl, and A. W. M. Mitchell, *Gray's Basic Anatomy*, 3rd ed., Elsevier, Chantilly, pp. 382-388, (2022).

[37] D. Hu, D. Howard, and L. Ren, "Biomechanical Analysis of the Human Finger Extensor Mechanism during Isometric Pressing," *PLoS One*, Vol. 9, No. 4, p. e94533, (2014).

[38] L. Wang, T. Meydan, and P. Williams, "A Two-Axis Goniometric Sensor for Tracking Finger Motion," *Sensors*, Vol. 17, No. 4, p. 770, (2017).

[39] S. H. Kim *et al.*, "Three-Dimensional Magnetic Rehabilitation, Robot-Enhanced Hand-Motor Recovery after Subacute Stroke: A Randomized Controlled Trial,"*Brain Sci.,* Vol. 13, pp. 1685, (2023).

[40] J. Lenarcic, T. Bajd, and M. M. Stanišić, *Robot mechanisms*, Springer Dordrecht, Dordrecht, pp. 313-326, (2012).

[41] Abie Salamat Orthopedic Co., "Neoprene Wrist Support with Splint," Abie Salamat Online Medical Store. Accessed: Nov. 04, 2025. [Online].

[42] A. Yu, K. L. Yick, S. P. Ng, and J. Yip, "2D and 3D anatomical analyses of hand dimensions for custom-made gloves," *Appl. Ergon.*, Vol. 44, No. 3, pp. 381–392, (2013).

[43] S. Cobos, M. Ferre, M. A. Sanchez Uran, J. Ortego, and C. Pena, "Efficient human hand kinematics for manipulation tasks," *2008 IEEE/RSJ International Conference on Intelligent Robots and Systems*, Nice, France, pp. 2246–2251, (2008).

[44] J. Li, R. Zheng, Y. Zhang, and J. Yao, "iHandRehab: An interactive hand exoskeleton for active and passive rehabilitation," *2011 IEEE International Conference on Rehabilitation Robotics*, Zurich, Switzerland, pp. 1–6, (2011).

[45] T. Ahmed *et al.*, "Flexohand: A Hybrid Exoskeleton-Based Novel Hand Rehabilitation Device," *Micromachines*, Vol. 12, No. 11, p. 1274, (2021).

[46] N. Sun, G. Li, and L. Cheng, "Design and Validation of a Self-Aligning Index Finger Exoskeleton for Post-Stroke

Rehabilitation," *IEEE Trans. Neural Syst. Rehabil. Eng.*, Vol. 29, pp. 1513–1523, (2021).

[47] C. J. W. Haarman, E. E. G. Hekman, J. S. Rietman, and H. Van Der Kooij, "Mechanical Design and Feasibility of a Finger Exoskeleton to Support Finger Extension of Severely Affected Stroke Patients," *IEEE Transactions on Neural Systems and Rehabilitation Engineering*, Vol. 31, pp. 1268–1276, (2023).

[48] M. Blackburn, P. van Vliet, and S. P. Mockett, Reliability of Measurements Obtained With the Modified Ashworth Scale in the Lower Extremities of People With Stroke," *Phys. Ther.*, Vol. 82, No. 1, pp. 25–34, (2002).

How to cite this paper:

B. Sarikhani, M. A. Ahmadi-Pajouh, A. Kolivand and F. Bakhtiari-Nejad, "Design and fabrication of an exoskeleton for the rehabilitation of hand fingers", *J. Comput. Appl. Res. Mech. Eng.*, Vol. 15, No. 1, pp. 17-38, (2025).

DOI: : 10.22061/jcarme.2025.11546.2542

URL: https://jcarme.sru.ac.ir/?_action=showPDF&article=2452